Development/Plasticity/Repair

Postsynaptic NMDA Receptor Expression Is Required for Visual Corticocollicular Projection Refinement in the Mouse Superior Colliculus

Kristy O. Johnson,[1,2] Leeor Harel,[1] and Jason W. Triplett[1,2,3,4]

[1]Center for Neuroscience Research, Children's National Research Institute, Washington, DC 20010, [2]Institute for Biomedical Sciences, George Washington University School of Medicine, Washington, DC 20037, [3]Department of Pediatrics, George Washington University School of Medicine, Washington, DC 20037, and [4]Department of Pharmacology and Physiology, George Washington University School of Medicine, Washington, DC 20037

Efficient sensory processing of spatial information is facilitated through the organization of neuronal connections into topographic maps of space. In integrative sensory centers, converging topographic maps must be aligned to merge spatially congruent information. The superior colliculus (SC) receives topographically ordered visual inputs from retinal ganglion cells (RGCs) in the eye and layer 5 neurons in the primary visual cortex (L5-V1). Previous studies suggest that RGCs instruct the alignment of later-arriving L5-V1 inputs in an activity-dependent manner. However, the molecular mechanisms underlying this remain unclear. Here, we explored the role of NMDA receptors in visual map alignment in the SC using a conditional genetic knockout approach. We leveraged a novel knock-in mouse line that expresses tamoxifen-inducible Cre recombinase under the control of the *Tal1* gene (*Tal1*^{CreERT2}), which we show allows for specific recombination in the superficial layers of the SC. We used *Tal1*^{CreERT2} mice of either sex to conditionally delete the obligate GluN1 subunit of the NMDA receptor (SC-cKO) during the period of visual map alignment. We observed a significant disruption of L5-V1 axon terminal organization in the SC of SC-cKO mice. Importantly, retinocollicular topography was unaffected in this context, suggesting that alignment is also disrupted. Time-course experiments suggest that NMDA receptors may play a critical role in the refinement of L5-V1 inputs in the SC. Together, these data implicate NMDA receptors as critical mediators of activity-dependent visual map alignment in the SC.

Key words: **alignment; map alignment; Tal1; topographic map; topography; visual**

Significance Statement

Alignment of topographic inputs is critical for integration of spatially congruent sensory information; however, little is known about the mechanisms underlying this complex process. Here, we took a conditional genetic approach to explore the role of NMDA receptors in the alignment of retinal and cortical visual inputs in the superior colliculus. We characterize a novel mouse line providing spatial and temporal control of recombination in the superior colliculus and reveal a critical role for NMDA expression in visual map alignment. These data support a role for neuronal activity in visual map alignment and provide mechanistic insight into this complex developmental process.

Introduction

The superior colliculus (SC) is a multisensory laminated structure in the midbrain that regulates eye and head movements during complex behaviors (May, 2006; Basso et al., 2021). In order to expedite sensory integration and decrease stimulus threshold, converging inputs to the SC are organized topographically and in alignment with one another (Basso and May, 2017; Johnson and Triplett, 2021). For instance, the SC receives visual input from retinal ganglion cells (RGCs) in the eye and layer 5 neurons in the primary visual cortex (L5-V1), each of which are organized topographically and in register (Triplett et al., 2009; Wang and Burkhalter, 2013). The establishment of aligned visual maps in

Received Aug. 1, 2022; revised Nov. 9, 2022; accepted Nov. 13, 2022.

Author contributions: K.O.J., L.H., and J.W.T. performed research; K.O.J., L.H., and J.W.T. analyzed data; K.O.J. wrote the first draft of the paper; J.W.T. designed research; J.W.T. edited the paper; J.W.T. wrote the paper.

This work was supported by National Institutes of Health, National Eye Institute Grant R01 EY025267 to J.W.T.; and National Institute of Child Health and Human Development District of Columbia Intellectual and Developmental Disabilities Research Center DC-IDDRC Award P50HD105328 by (PI: V. Gallo). We thank members of the Joshua Corbin, Michael Sidorov, and Michael Shoykhet laboratories for helpful discussion; and David Feldheim for comments on the manuscript.

The authors declare no competing financial interests.

Correspondence should be addressed to Jason W. Triplett at jtriplett@childrensnational.org.

https://doi.org/10.1523/JNEUROSCI.1473-22.2022

the mouse SC occurs over the first two postnatal weeks. First, RGCs innervate the SC beginning just before birth and are guided to their mature termination zones (TZs) by the end of the first postnatal week (McLaughlin et al., 2003). Second, axons of L5-V1 neurons enter the SC beginning around postnatal day 6 (P6) and refine to their final TZs in alignment with the previously established retinocollicular map by P12 (Triplett et al., 2009). Previous studies suggest that retinal inputs in the SC instruct the topographic alignment of L5-V1 terminals (Triplett et al., 2009); however, the underlying mechanisms remain unclear.

Two models have been put forth to explain how RGCs instruct L5-V1 alignment. The first hypothesizes that molecular cues, specifically ephrin-A family members, expressed by both RGCs and cells in the SC guide L5-V1 axons to terminate appropriately (Savier et al., 2017, 2020). Indeed, it is well established that graded expression of ephrin-As along the anterior-posterior (A-P) axis of the SC is necessary for establishing retinocollicular topography. In this model of visual map alignment, ephrin-As expressed by innervating RGCs modify the existing collicular ephrin-A gradient, which is then used by later-arriving L5-V1 axons to sort topographically. In support of this, overexpression of ephrin-A3 in a subset of RGCs results in aberrant L5-V1 topography (Savier et al., 2017); and computational models of predicted gradient alterations are consistent with these observations (Savier et al., 2020).

The second model of retinal instruction of visual map alignment posits that spontaneous neuronal activity serves as the driving force. Here, coincident activity of L5-V1 neurons and RGCs originating from topographically congruent regions drives synaptic strengthening in postsynaptic SC neurons. In support of this model, genetic disruption of spontaneous cholinergic retinal waves impairs L5-V1 alignment in the SC (Triplett et al., 2009). Consistent with this, computational modeling of altered wave activity revealed similar results and suggested an integrative mechanism of activity-dependent alignment was feasible (Tikidji-Hamburyan et al., 2016). However, the underlying mechanisms of activity-driven map alignment remain unclear.

NMDARs are glutamatergic receptors that play important roles in synaptic plasticity, arbor stabilization, and axonal refinement (Nicoll and Malenka, 1999; Kutsarova et al., 2016). Furthermore, NMDARs play a role in visual system development, specifically regulating the development of retinocollicular/retinotectal topography (Cline and Constantine-Paton, 1989; Simon et al., 1992) and developmental plasticity of retinotectal circuits (Kesner et al., 2020). Together, these data suggest that NMDARs may be ideally positioned to mediate activity-driven visual map alignment in the SC.

Here, we took a conditional genetic approach to determine the role of SC-expressed NMDARs in visual map alignment. To do so, we leveraged a novel mouse line ($Tal1^{CreERT2}$), which allowed for temporal control of recombination with spatial restriction to neurons in the midbrain, particularly the superficial SC (sSC). We deleted the obligate *GluN1* subunit of NMDARs in the midbrain beginning after retinocollicular map formation. Anatomical tracing experiments revealed an enlarged terminal field of labeled L5-V1 axons in the SC, but no effect on retinocollicular nor retinogeniculate topography. Furthermore, time-course experiments suggest deficits in L5-V1 axonal refinement in the absence of NMDAR function. Together, these data suggest that NMDARs expressed by neurons in the SC are required for visual corticocollicular projection refinement and map alignment and may serve as the mechanistic underpinning of activity-dependent retinal instruction of this process.

Materials and Methods

Mice. The $Tal1^{CreERT2}$ transgenic mouse line was generated by Cyagen and genotyped with two allele-specific primers (forward: GAG-AGA-ACT-AAT-TGT-CAG-CAG-G; and reverse: ATC-TTT-GTC-TGC-ACA-CTT-GG). Briefly, the $Tal1^{CreERT2}$ constitutive knock-in mouse was generated by replacing the TGA stop codon with a "2A-CreERT2" cassette conferring neomycin resistance (Neo^r) (see Fig. 1*A*). The Neo portion of the cassette was flanked by self-deletion anchors, allowing for removal after germline targeting. Mice harboring a floxed allele of the *Grin1* gene ($GluN1^{flox}$) were generated and genotyped as described previously (Tsien et al., 1996). Adult and juvenile mice of either sex were used. Their ages ranged between postnatal days (P) 5-45. All animals were housed in the research animal facility at Children's National Research Institute, and all experimental procedures were approved by the Institutional Animal Care and Use Committee.

X-gal staining. Adult animals were anesthetized with halothane and intracardially perfused ice-cold PBS followed by 4% PFA in PBS, pH 7.4. Eyes and brains were dissected and postfixed 30 min or 2 h in 4% PFA, respectively. Retinas were dissected from eyes and prepared for flat mount by making relieving cuts into the optic cup. Retinas and brain sections were washed 3 times in LacZ Wash Buffer (0.1 M $NaPO_4$, pH 7.4, 2 mM $MgCl_2$, 0.02% (v/v) IGEPAL, 0.01% sodium deoxycholate) before incubation overnight at room temperature in staining buffer (Wash Buffer + 5 mM $K_4Fe(CN)_6$, 5 mM $K_3Fe(CN)_6$, and 1 mg/ml X-gal (Sigma)). Images were acquired on Zeiss Lumar microscope with an Axiocam HRc camera (Zeiss) and Axiovision (4.6) software.

Immunohistochemistry. Mice were anesthetized on ice (<P8) or with halothane (2-bromo-2-chloro-1,1,1-trifluoroethane) (>P9) and transcardially perfused with ice-cold PBS followed by 4% PFA in PBS, pH 7.4. Brains were dissected and postfixed in 4% PFA at 4°C overnight. After postfixation, brains were briefly washed in PBS before embedding in 2% agarose in PBS for sectioning on a VT1000 vibratome (Fisher Scientific). Tissue was sectioned at 75 µm and collected in PBS for staining. Sections were incubated in blocking solution (1% serum, 0.25% Triton X-100) for 1 h at room temperature and then incubated with primary antibodies diluted in blocking solution at 4°C for 2-3 d. The following primary antibodies were used: Anti-Tal1 (Novus Bio NBP2-59 207, RRID:AB_2921337, 1:1000), Anti-NeuN (Abcam AB177487, RRID:AB_2532109, 1:2000), Anti-Neurogranin (Abcam AB5620, RRID:AB_91937, 1:500), Anti-Parvalbumin (Swant PV 27, RRID:AB_2631173, 1:1000), Anti-Gad67 (Millipore MAB5406, RRID:AB_2278725, 1:500), Anti-Reelin (Abcam AB78540, RRID:AB_1603148, 1:500), and Anti-tdTomato (Origene AB8181-200, RRID:AB_2722750, 1:2000). Sections were washed thoroughly in PBS and then incubated with appropriate secondary antibodies (Biotium #20016, #20039, and #20172, RRID:AB_10563028, RRID:AB_10556967, and RRID:AB_10871469, respectively, 1:1000) and DAPI diluted in blocking solution for 1 h at room temperature. Sections were washed thoroughly, mounted onto glass slides, and coverslipped with Fluoromount-G (Fisher Scientific). Images were acquired at 20× magnification on an Olympus FV1000 confocal microscope with an Olympus DP71 digital camera attached. Images were analyzed and processed with FIJI (Schindelin et al., 2012).

qPCR. Total RNA was isolated from micro-dissected SC and V1 using the Aurum Total RNA Fatty and Fibrous Tissue Kit (Bio-Rad #7326830). Synthesis of cDNA was conducted using the iScript Reverse Transcription Supermix for qRT-PCR (Bio-Rad). qPCR was performed on a CFX96 real-time system (Bio-Rad #1708890) in a 20 µl reaction mixture using SsoAdvanced Universal SYBR Green PCR master mix (Bio-Rad). Cycle parameters were 3 s at 95°C and 30 s at 60°C. Data were normalized to housekeeping gene 18S. *18S* primers: 5′-CTTTGTCAA GCTCATTTCCTGG-3′ and 5′-TCTTGCTCAGTGTCCTTGC-3′; *GluN1* primers: set 1: 5′-CCAGATGTCCACCAGACTAAA −3′ and 5′-CCATT GACTGTGAACTCCTCTT-3′, set 2: 5′-AAGGAGTGGAACGGAATGA TG-3′ and 5′-GGCTTGGAGAACTCTATGTACTG-3′, set 3: 5′-GTAGCT GGGATCTTCCTCATTT-3′ and 5′-TTCTTCCTCCACACGTTCAC-3′.

Anterograde RGC axon labeling. Neonatal pups aged postnatal day 6 (P6), P8 or P10 were anesthetized on ice. For focal labeling of RGCs, a 10% solution of lipophilic dye DiI (1,1′-dioctodecyl-

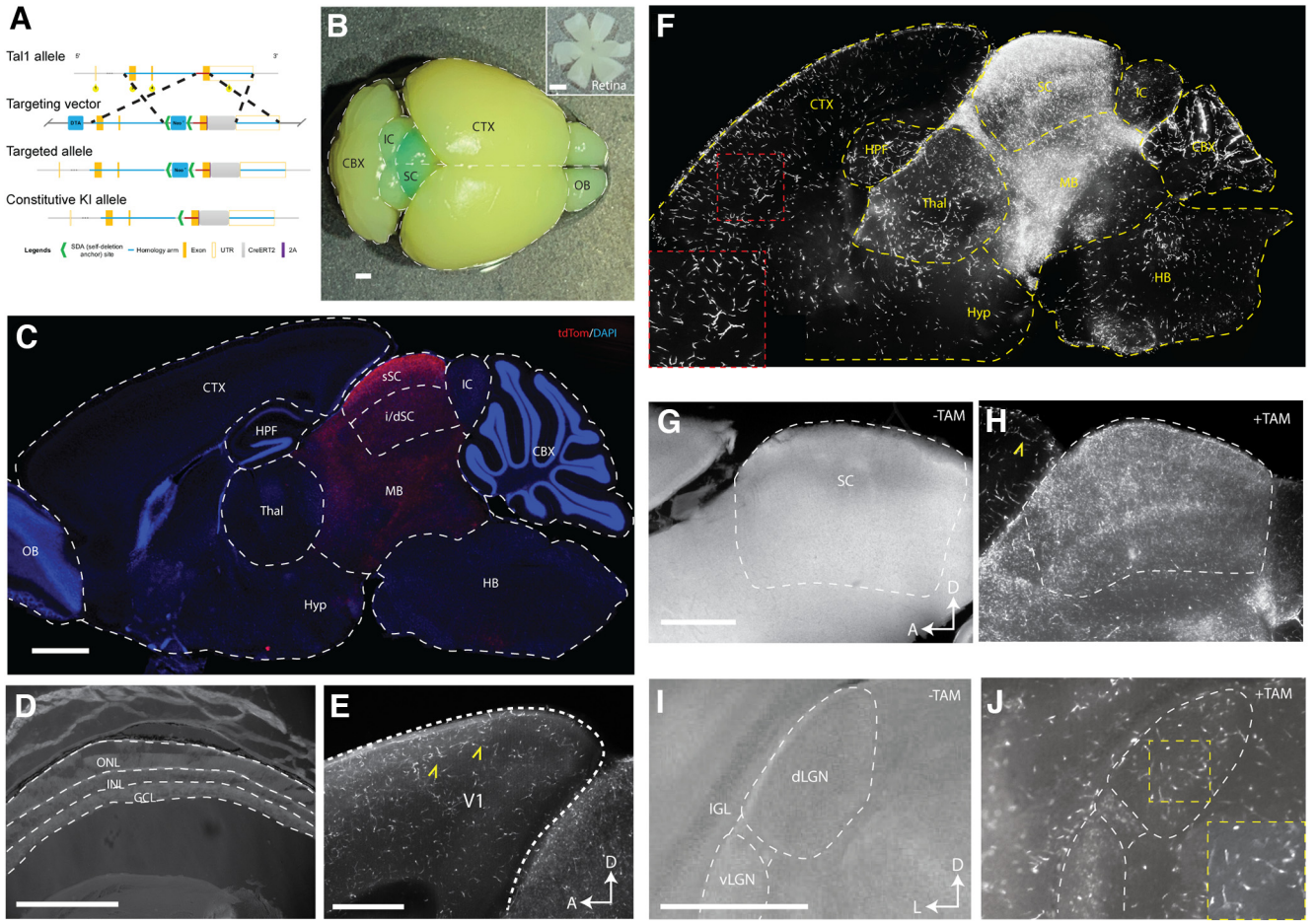

Figure 1. *Tal1*^{CreERT2} mice allow for specific recombination in the midbrain. ***A***, Schematic of WT allele of *Tal1* gene locus on chromosome 4 of the mouse and targeting construct for the constitutive knock-in of tamoxifen-inducible Cre recombinase (Cre^{ERT2}) into the 3′ untranslated region. ***B***, Whole-mount views of X-gal-stained brain and retina (inset) from a P21 *Tal1*^{CreERT2};*Rosa*^{LacZ} reporter mouse administered tamoxifen from P6 to P8 reveals specific recombination in the midbrain. Scale bar, 250 μm. ***C***, Parasagittal section through the brain of a P21 *Tal1*^{CreERT2};*Rosa*^{tdTom} reporter mouse administered tamoxifen from P6 to P8 reveals concentrated recombination in the sSC. Scale bar, 500 μm. CBX, Cerebellar cortex; CTX, cerebral cortex; HB, hindbrain; HPF, hippocampal formation; Hyp, hypothalamus; IC, inferior colliculus; MB, midbrain; OB, olfactory bulb; i/dSC, intermediate/deep SC; Thal, thalamus. ***D***, Section through the retina of a P12 *Tal1*^{CreERT2};*Rosa*^{tdTom} reporter mice administered tamoxifen from P6 to P8 reveals no recombination. Scale bar, 500 μm. ONL, Outer nuclear layer; INL, inner nuclear layer; GCL, ganglion cell layer. ***E***, Magnified image of primary visual cortex (V1) from the image shown in (***F***) reveals recombination in V1 is limited to vasculature (yellow carats). Scale bar, 500 μm. ***F***, Overexposed parasagittal section through the brain of a P12 *Tal1*^{CreERT2};*Rosa*^{tdTom} reporter mouse administered tamoxifen from P6 to P8 reveals additional signal in regions outside of the midbrain that appear to be limited to vasculature (red dashed box and inset). ***G***, ***H***, Magnified images of the SC from P12 *Tal1*^{CreERT2};*Rosa*^{tdTom} reporter mice administered vehicle (peanut oil) (***G***) or tamoxifen (***H***) from P6 to P8 reveals specific recombination on drug administration. Yellow carats represent putative vasculature staining. Scale bar, 500 μm. ***I***, ***J***, Coronal sections through the brains of P12 *Tal1*^{CreERT2};*Rosa*^{tdTom} reporter mice administered vehicle (peanut oil) (***I***) or tamoxifen (***J***) from P6 to P8 reveal specific recombination on drug administration. Recombination in the dorsal LGN (dLGN) appears to be limited to vasculature (yellow carats, inset). Scale bar, 500 μm. IGL, Intergeniculate leaflet; vLGN, ventral LGN.

3,3,3′,3′-tetramethyllindocarbocyanine perchlorate) in dimethylformamide was injected using a pulled-glass micropipette attached to a Picospritzer III (Parker-Hannifin). The glass micropipette was inserted into the retina of the anesthetized animal, and ~100 nl of DiI solution was injected into one eye. For corticocollicular axon tracing, the skull was exposed, and the glass micropipette inserted through the skull of the anesthetized animal; ~100 nl of DiI solution was injected into the primary visual cortex. All animals were warmed at 37°C for 30–45 min before being placed back into their home cage. All pups recovered for 2 d before tissue harvesting and their brains postfixed in 4% PFA overnight as described above. The TZs of DiI-labeled retinocollicular neurons in the SC were visualized in whole mount via epifluorescent microscopy. Brains were then embedded in 3% agarose and sectioned in the coronal plane (for retinogeniculate tracings) or sagittal plane (for corticocollicular tracings) at 100 μm on a VT1000 vibratome (Fisher Scientific). The dLGN and SC were visualized at 1.25× and 4× magnification with BX63 Olympus Microscope and analyzed on FIJI.

Image analysis. To determine topographic refinement of retinofugal TZs, we calculated a TZ index (TZI), for which the size of the TZ in the SC or dLGN, expressed as a percent of the target area, was divided by the injection size, expressed as a percent of the flat-mounted retina. For the dLGN, we quantified the TZI for all sections containing the TZ and determined an average across sections for each animal. The boundaries of the dLGN/SC were outlined on a grayscale 8-bit image, and the background was cleared before measuring the size of the dLGN/SC. For corticocollicular projections, we calculated the size of the TZ as a percent of the total SC in sagittal sections. All sections containing the TZ were quantified and averaged to obtain a single value per injection.

Experimental design and statistical analysis. For immunohistochemical analyses in Figure 3, we averaged the number of counted cells over three different SC sections from each of 3 animals. For qPCR in Figure 4, data were analyzed using the comparative CT method (Schmittgen and Livak, 2008); and statistical significance was determined using a two-way ANOVA with Sidak's multiple comparisons test. For retinocollicular and corticocollicular tracings at P12 (see Figs. 5 and 6), TZ sizes were statistically analyzed using an unpaired Student's *t* test. For corticocollicular tracings at P8 and P10 (see Fig. 7), a two-way ANOVA with Sidak's multiple comparisons test was used to determine effects of age and genotype. All statistical analyses were performed with Prism 9.4.1 (GraphPad).

Results

Tal1^{CreERT2} mice allow for temporally regulated recombination in the sSC

In order to determine the role of NMDARs in visual map alignment in the SC, we developed a tamoxifen-inducible Cre line that would allow us to manipulate gene expression in the SC with temporal control. Based on previous reports (Bradley et al., 2007) and publicly available expression data from the Allen Brain Atlas, we identified *Tal1* as a candidate gene to drive expression of Cre recombinase specifically in the sSC. *Tal1* is a basic helix-loop-helix transcription factor expressed in hematopoietic, vascular, and midbrain neuronal lineages (Elefanty et al., 1999; van Eekelen et al., 2003). Thus, we targeted the *Tal1* locus for specific knock-in of a CreERT2 construct into the 3′ untranslated region generating *Tal1*^{CreERT2} mice (Fig. 1*A*).

To characterize the pattern of recombination in *Tal1*^{CreERT2} mice, we crossed this line with β-galactosidase (*Rosa*^{LacZ}) or tdTomato (*Rosa*^{tdTom}) reporter mice (Soriano, 1999; Madisen et al., 2010). Since our goal was to induce recombination during the period of visual map alignment, we administered tamoxifen daily from P6 to P8 and analyzed reporter expression at P10. Whole-mount staining of *Tal1*^{CreERT2};*Rosa*^{LacZ} reporter brains revealed strong signal almost exclusively in the SC and notably absent from the cerebral cortices (Fig. 1*B*), consistent with previous transgenic lines driving LacZ expression under the control of *Tal1* promoter elements (Elefanty et al., 1999; Bradley et al., 2007). Analysis of parasagittal sections in *Tal1*^{CreERT2};*Rosa*^{tdTom} reporter mice revealed that expression extended from the sSC dorsally through the substantia nigra ventrally and from the pretectum anteriorly to the cuneiform nucleus posteriorly. Importantly, no signal was observed in vehicle-treated controls (Fig. 1*G–I*), suggesting tight regulation of recombination in response to tamoxifen administration.

We observed strong signal in the sSC (Fig. 1*C*,*H*), suggesting broad expression in regions receiving visual inputs. Of note, overexposure of tdTom signal revealed expression in other regions of the brain, including the cortex, cerebellum, and thalamus; however, signal in these regions appeared to be mainly in the pattern of blood vessels (Fig. 1*E*,*F*,*J*), consistent with the role Tal1 plays in the genesis of endothelial cells (Göthert et al., 2005). We carefully inspected expression in the retina but did not observe expression using either reporter line (Fig. 1*B*,*D*). To rule out the possibility that gene expression might be altered along the retinogeniculocortical pathway, we examined recombination in the lateral geniculate nucleus (LGN). Interestingly, we observed neuropil-like expression in the ventral LGN and intergeniculate leaflet, but not in the dorsal LGN, where the pattern was blood vessel-like (Fig. 1*J*). Together, these data suggest that *Tal1*^{CreERT2} mice allow for inducible recombination broadly in the midbrain, including prominently in the sSC, but not in visual afferent projection areas to the SC, specifically RGCs or L5-V1 neurons.

We next determined the range of ages during which Cre recombination could be induced in *Tal1*^{CreERT2};*Rosa*^{tdTom} mice. We injected 250 µg tamoxifen intragastrically at P0, P5, P10, P15, P20, and P30 and analyzed expression at P5, P10, P15, P20, P30, and P45, respectively. The most robust expression of tdTom-expressing cells was observed in animals injected at P0, P5, and P10 (Fig. 2*A–C*). In older juvenile animals (P15, P20, and P30), injections were administered intraperitoneally, and a reduction in the proportion of labeled cells was noticeable (Fig. 2*D–F*). This is likely because of the relatively lower dose administered at these ages, since we gave the same absolute amount of tamoxifen. Of note, however, substantial numbers of cells in the sSC were labeled at each age, suggesting that *Tal1*^{CreERT2} mice could be used for gene manipulation over a long developmental window. Overall, these results demonstrated that Cre-mediated recombination is induced with a single injection of tamoxifen at all ages, although the proportion of cells labeled reduced with age, as the relative dose decreased.

Tal1^{CreERT2} marks a subset of neurons in the sSC

To determine the complement of cells marked in this new line, we injected *Tal1*^{CreERT2};*Rosa*^{tdTom} reporter mice with tamoxifen daily from P6 to P8 and analyzed expression of various cell type-specific markers by immunohistochemistry at P21. We focused specifically on the sSC, since this is the region innervated by RGCs and L5-V1 axons. To begin, we asked how faithfully the *Tal1*^{CreERT2} line replicated endogenous expression of Tal1. As expected, based on our knock-in targeting design, we found that the vast majority of tdTom$^+$ cells were also Tal1$^+$ (84.4 ± 1.3%, $N = 3$) (Fig. 3*A*,*H*). Similarly, nearly all Tal1$^+$ neurons were marked with tdTom (87.5 ± 0.7%, $N = 3$) (Fig. 3*A*,*H*), suggesting highly efficient induction of recombination by tamoxifen treatment. Next, we found that nearly all cells marked in the sSC of *Tal1*^{CreERT2} mice were neurons, as indicated by expression of the neural nuclear antigen NeuN (81.5 ± 2.9%, $N = 3$) (Fig. 3*B*,*H*). Intriguingly, these represent a substantial proportion of all neurons in the sSC (28.1 ± 1.7%, $N = 3$), although the majority of neurons in the sSC were not labeled in *Tal1*^{CreERT2} reporter mice. We hypothesized that the remainder of marked cells in the sSC may be astrocytes; however, few, if any, tdTom$^+$ cells were colabeled with S100β (Fig. 3*C*,*H*).

Given the high proportion of neurons marked in *Tal1*^{CreERT2} mice, we next sought to determine the subtype of neurons labeled by this line. Recent work suggests that *Tal1* expression may be associated with inhibitory fates (Morello et al., 2020). We did not observe a high degree of colocalization of Gad67 with tdTom$^+$ neurons in the sSC of *Tal1*^{CreERT2} reporter mice (Fig. 3*G*). However, we did observe that a substantial proportion of tdTom$^+$ cells were also positive for reelin (31.0 ± 2.8%, $N = 3$) (Fig. 3*D*,*H*), which is expressed by a subset of GABAergic neurons in other brain regions (Ramos-Moreno et al., 2006). Interestingly, we did not observe colocalization with other known inhibitory markers, such as parvalbumin or neurogranin (Fig. 3*E*, *F*,*H*). Together, these data suggest that the *Tal1*^{CreERT2} line enables recombination in a substantial portion of neurons in the sSC, which are likely comprised of a mixture of excitatory and inhibitory subtypes.

SC-specific loss of *GluN1* expression in *Tal1*^{CreERT2}; *GluN1*$^{flox/flox}$ mice

To test our hypothesis that NMDARs expressed in the SC mediate visual map alignment, we crossed *Tal1*^{CreERT2} mice with a line harboring a floxed allele of the *GluN1* gene coding for the obligate subunit of the NMDAR (*GluN1*^{fl}), in which exon 11 through the 3′ end is flanked by loxP sites (Tsien et al., 1996). We refer to mice genotyped as *Tal1*^{CreERT2};*GluN1*$^{fl/fl}$ as SC-cKO animals, whereas those with a genotype of *Tal1*$^{+/+}$;*GluN1*$^{fl/+}$ or *Tal1*$^{+/+}$;*GluN1*$^{fl/fl}$ were considered control littermates (Ctl). All mice were administered tamoxifen, and heterozygous cKO animals (*Tal1*^{CreERT2};*GluN1*$^{fl/+}$) were not included in our analyses.

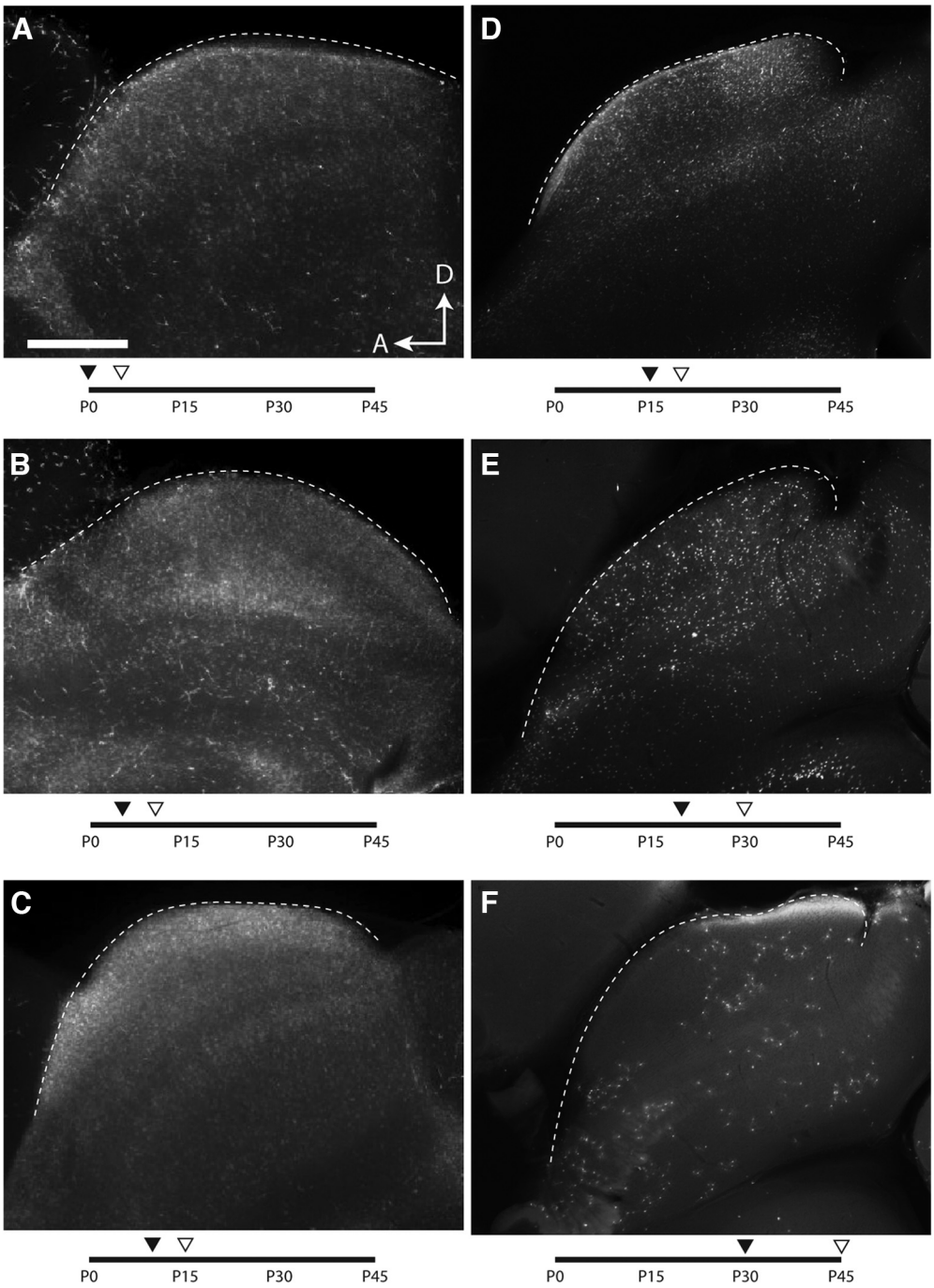

Figure 2. Induction of *Tal1*^{CreERT2} mediated recombination throughout development. ***A–F***, Parasagittal sections through the SC of *Tal1*^{CreERT2};*Rosa*^{tdTom} reporter mice administered tamoxifen (black triangles) and analyzed (open triangles) at the ages indicated in the timeline below each panel. Drug administration induces recombination at all ages tested. Scale bar, 500 μm. A, Anterior; D, dorsal.

To determine the degree to which *GluN1* expression was reduced in SC-cKO mice, we performed qRT-PCR using primer sets against the floxed region of the gene (Fig. 4*A*). All animals were intragastrically injected with tamoxifen daily from P6 to P8 and analysis performed at P10. We found a main effect of genotype on the expression of GluN1 transcript in the SC of SC-cKO mice ($p < 0.0001$, two-way ANOVA, $N > 8$), and *post hoc* analyses indicated a significant decrease in all three primer sets in SC-cKO mice compared with controls ($p < 0.0001$, Sidak's multiple comparison test) (Fig. 4*B*). Similar analyses did not reveal an effect of genotype for *GluN1* expression in V1 ($p = 0.4966$, two-way ANOVA, $N > 8$), suggesting that knockdown of expression is restricted to the SC in SC-cKO mice (Fig. 4*C*).

Retinocollicular and retinogeniculate map organization is unaltered in SC-cKO mice

Given that previous studies indicate that retinal inputs instruct L5-V1 terminals (Triplett et al., 2009; Savier et al., 2017), we next analyzed retinocollicular map organization following ablation of GluN1 in the SC during the second postnatal week. To begin, Ctl and SC-cKO animals were administered tamoxifen from P6 to P8, and a small amount of the lipophilic tracer DiI was injected

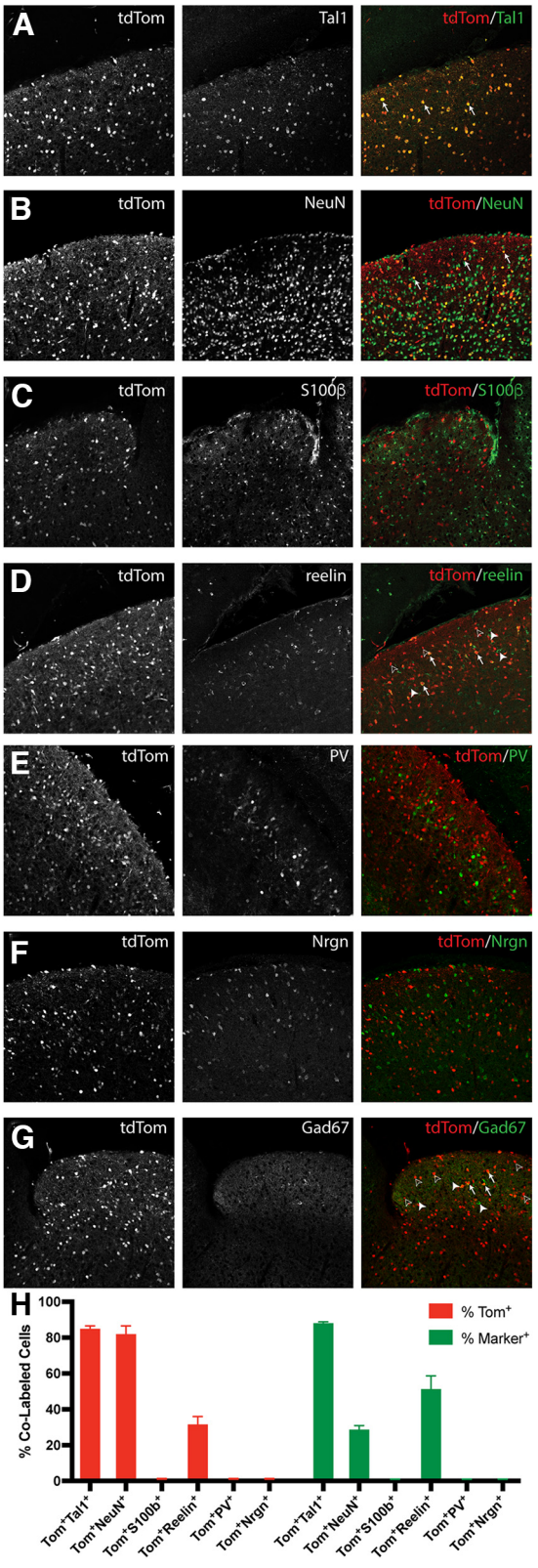

Figure 3. Recombination in a subset of neurons in the SC of *Tal1*^{CreERT2} mice. ***A-G***, Parasagittal sections through the SC of P21 *Tal1*^{CreERT2};*Rosa*^{tdTom} reporter mice administered tamoxifen from P6 to P8 costained to reveal cells expressing Tal1 (***A***), neurons expressing NeuN (***B***), astrocytes expressing S100β (***C***), and neurons expressing reelin (***D***), parvalbumin (PV) (***E***), neurogranin (Nrgn) (***F***), or Gad67 (***G***). ***H***, Quantification of the proportion of tdTom-positive (red) or marker-positive (green) that were both tdTom- and marker-positive reveals that a high proportion of *Tal1*^{CreERT2}-labeled cells express Tal1 and NeuN and a prominent subset express reelin, while little overlap was observed with other markers. Data are mean ± SD.

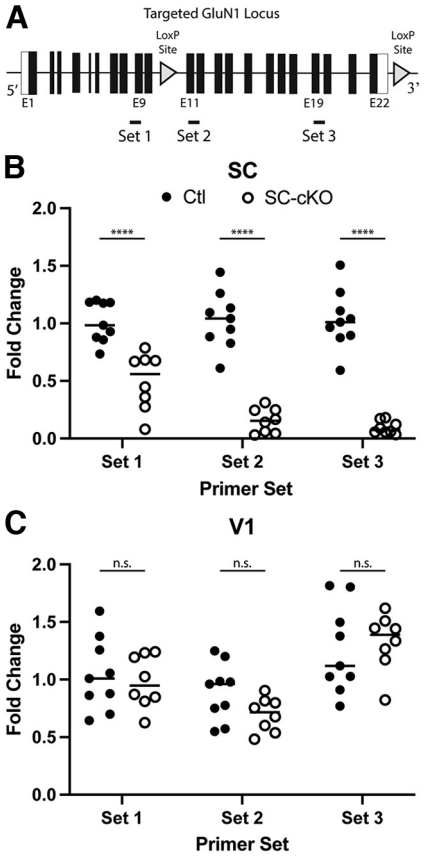

Figure 4. Efficient knockdown of *GluN1* in *Tal1*^{CreERT2};*GluN1*$^{fl/fl}$ mice. ***A***, Schematic showing the targeted *GluN1* gene locus in floxed mice and the approximate location of the *GluN1* probe sets used for qPCR. ***B***, ***C***, Quantification of the fold change in *GluN1* expression in the SC (***B***) and V1 (***C***) of P10 *Tal1*^{CreERT2};*GluN1*$^{fl/fl}$ mice administered tamoxifen from P6 to P8 reveals a significant decrease in transcript expression in the SC but not V1. Lines indicate median. ****$p < 0.0001$, two-way ANOVA with Sidak's multiple comparisons test.

into the retina at P10. To assess retinocollicular topography, TZs in the SC were visualized in whole mount at P12 (Fig. 5*A–C*). Qualitatively, we observed no difference in TZ organization, and quantification of the TZI did not reveal any differences between groups (Ctl: 1.179 ± 0.1858, $N = 16$; SC-cKO: 1.332 ± 0.2014, $N = 11$; $p = 0.5886$, Student's t test) (Fig. 5*D*). These data suggest that NMDAR function in the SC is not required after the first postnatal week to maintain retinocollicular axon refinement.

We next wanted to assess topography along the retinogeniculate pathway, since alterations may affect topography in V1 (Cang et al., 2005); and we observed recombination in the dLGN of *Tal1*^{CreERT2} reporter mice, although it appeared to be restricted to blood vessels (Fig. 1*E,F,H,J*). We visualized TZs in the dLGN in coronal sections and calculated the TZI. Similar to retinocollicular tracings, we did not observe qualitative or quantitative changes in TZI between groups (Ctl: 8.261 ± 0.9520, $n = 11$; SC-cKO: 6.538 ± 0.7098, $n = 11$; $p = 0.1621$, Student's t test) (Fig. 5*E–H*). Together, these data show that ablating *GluN1* expression in the SC during the second postnatal week did not affect retinocollicular nor retinogeniculate map refinement.

NMDAR function in the SC is required for corticocollicular topography

Having established that *GluN1* expression is knocked down in the SC of *Tal1*^{CreERT2};*NR1*$^{fl/fl}$ mice and this does not impact topography along the retinocollicular nor retinogeniculate

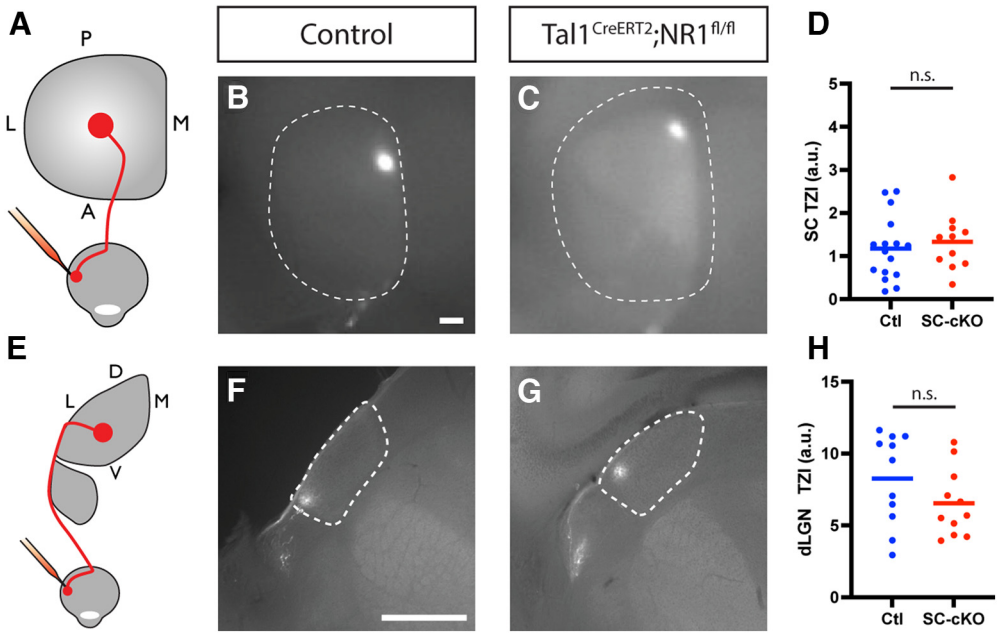

Figure 5. Retinofugal topography is unaffected in *GluN1* SC-cKO mice. ***A***, Schematic of retinocollicular tracing strategy. ***B***, ***C***, Whole-mount views of retinocollicular TZs in the SCs of P12 control (***B***) and *Tal1*^{CreERT2};*GluN1*$^{fl/fl}$ (***C***) mice administered tamoxifen from P6 to P8. Scale bar, 250 µm. ***D***, Quantification of TZI in the SC reveals no difference between groups. $p = 0.5886$, Student's *t* test. ***E***, Schematic of retinogeniculate tracing strategy. ***F***, ***G***, Coronal sections through the dLGNs of P12 control (***F***) and *Tal1*^{CreERT2};*GluN1*$^{fl/fl}$ (***G***) mice administered tamoxifen from P6 to P8 to reveal TZs. Scale bar, 250 µm. ***H***, Quantification of TZI in the dLGN reveals no difference between groups. Lines indicate median. $p = 0.1621$, Student's t test.

pathways, we could now test our hypothesis that NMDAR function is required for visual map alignment. To do so, we traced L5-V1 projections in Ctl and SC-cKO mice at P10 and visualized TZs in the SC at P12 (Fig. 6*A*–*C*). We found a significant increase in the TZ size of corticocollicular projections in the SC of SC-cKO mice compared with Ctl (Ctl: 8.44 ± 0.58, $N = 19$; SC-cKO: 14.58 ± 0.61, $N = 11$; $p < 0.0001$, Student's *t* test) (Fig. 6*D*). Intriguingly, we observed that a subset of TZs in SC-cKO mice appeared duplicated (45.4%, 5 of 11 mice) (Fig. 6*E*), a phenomenon we did not observe in Ctl animals (0.0%, 0 of 19 mice) (Fig. 6*F*). We next assessed whether these disruptions in TZ organization were because of alterations in the localization of projections within the SC. To do so, we plotted the TZ location along the A-P axis of the SC as a function of the injection site location along the lateral-medial (L-M) axis of V1 (Fig. 6*G*). In both groups, we observed a positive linear relationship indicating gross topographic order. We did not find a significant difference in the slopes of linear regression lines between groups (Ctl: 0.494; SC-cKO: 1.126, $p = 0.2731$), indicating that rough topographic mapping is not altered in SC-cKO mice. These data suggest that *GluN1* expression in Tal1^{+} neurons in the SC is required for refinement of L5-V1 projections, but not the establishment of rough topographic positioning. And, together with retinocollicular tracing data, these data suggest that visual map alignment is dependent on NMDAR function in the SC.

Postsynaptic expression of NMDARs in the SC is required for L5-V1 refinement

To further elucidate whether NMDAR function in the SC is required for initial targeting of terminal branches or their refinement, we examined L5-V1 projection organization over the course of development. Our previous work showed that L5-V1 axons enter the SC around P6 and refine to their mature state by P12 (Triplett et al., 2009). Thus, we focused on the P8 and P10 time points at which clear TZs could be identified that span the duration of refinement. Consistent with previous data, we found that L5-V1 terminals in Ctl mice formed poorly defined TZs at P8 with multiple stray arbors extending well beyond the borders of the primary TZ (Fig. 7*A*). We observed the same to be true in SC-cKO mice (Fig. 7*B*) and found no significant difference in TZ size between groups at P8 (Ctl: 12.79 ± 0.65, $N = 6$; SC-cKO: 14.41 ± 1.24, $N = 10$; $p = 0.3534$, Student's *t* test) (Fig. 7*E*). By P10, we observed fewer stray arbors outside the main TZ in both Ctl and SC-cKO mice; however, TZs appeared more condensed in Ctl SCs (Fig. 7*C*,*E*). Indeed, we found that TZs in SC-cKO mice were significantly larger than those in Ctl mice (Ctl: 9.83 ± 0.25, $N = 10$; SC-cKO: 13.55 ± 0.49, $N = 14$; $p < 0.0001$, Student's *t* test) (Fig. 7*D*,*E*), suggesting a failure to refine. To further test this possibility, we compared TZ sizes at P8 and P10 in both Ctl and SC-cKO mice. We found main effects of age ($p = 0.0194$, two-way ANOVA) and genotype ($p = 0.0016$), but no interaction between the two ($p = 0.1874$). Consistent with our previous analysis, *post hoc* tests revealed a significant difference in TZ size between Ctl and SC-cKO at P10 ($p = 0.001$, Sidak's multiple comparisons test), but not at P8 ($p = 0.345$). Interestingly, we also found a significant decrease in TZ size between P8 and P10 for Ctl mice ($p = 0.0401$), but not for SC-cKO mice ($p = 0.6205$). Together, these data suggest that NMDAR expression in the SC is critical for the refinement of L5-V1 axon terminals and alignment with the retinocollicular map.

Discussion

Previous studies suggest that activity plays an important role in the topographic alignment of corticocollicular projections with the already established retinocollicular map in the SC (Triplett et al., 2009). In this study, we explored the mechanisms by which activity mediates visual map alignment, focusing on NMDARs. We generated a mouse model that allowed for temporally

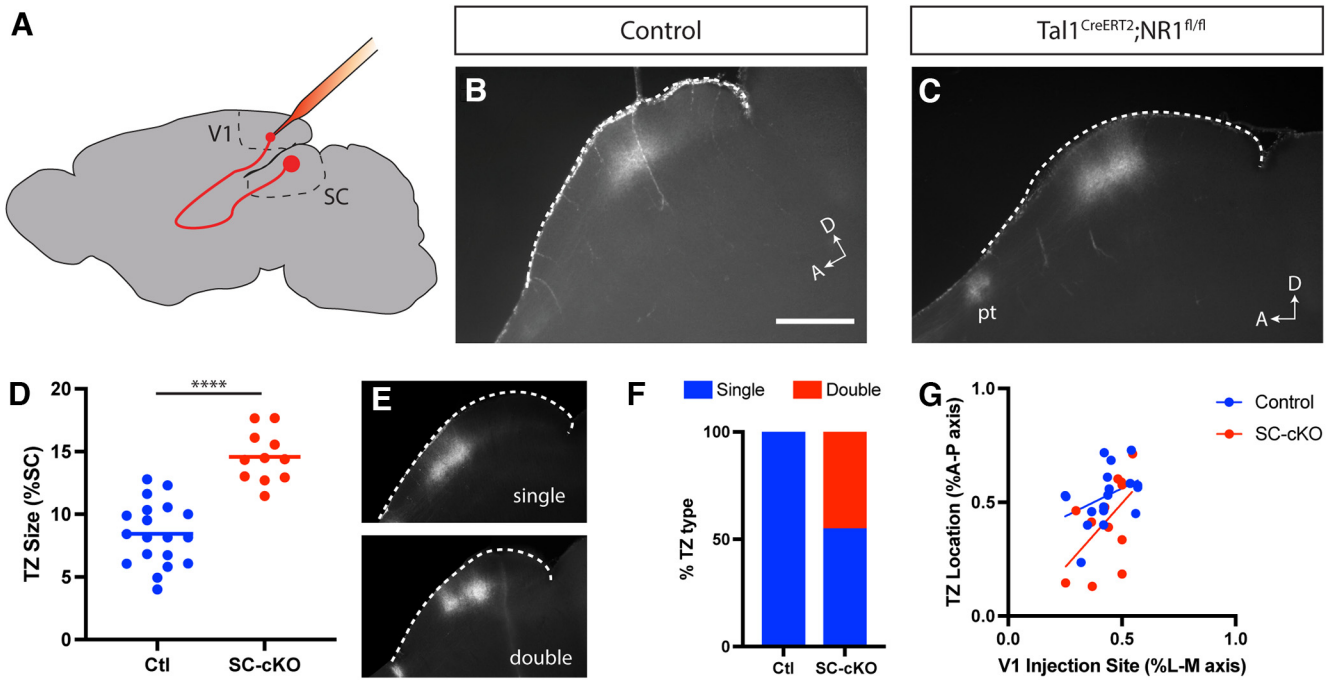

Figure 6. Disrupted corticocollicular topography in *GluN1* SC-cKO mice. ***A***, Schematic of corticocollicular tracing strategy. ***B***, ***C***, Parasagittal sections through the SCs of P12 control (***B***) and *Tal1*^{CreERT2};*GluN1*$^{fl/fl}$ (***C***) mice administered tamoxifen from P6 to P8 reveal TZs. Scale bar, 500 mm. A, Anterior; D, dorsal; pt, pretectum. ***D***, Quantification of TZ size measured as a percent of the sSC reveals a significant increase in *GluN1* SC-cKO mice. Lines indicate median. ****$p < 0.0001$, Student's *t* test. ***E***, Quantification of the corticocollicular TZ location along the A-P axis as a function of injection site along the lateral-medial (L-M) axis of the primary visual cortex (V1) reveals no significant change in topographic order (slope of linear regression, $p = 0.2731$). ***F***, Representative parasagittal sections from *Tal1*^{CreERT2};*GluN1*$^{fl/fl}$ mice in which corticocollicular TZs were classified as single (top) or double (bottom). ***G***, Quantification of the proportion of single and double TZs observed in reveals a substantial portion are double in SC-cKO mice (5 of 11), while none was observed in control mice (0 of 19).

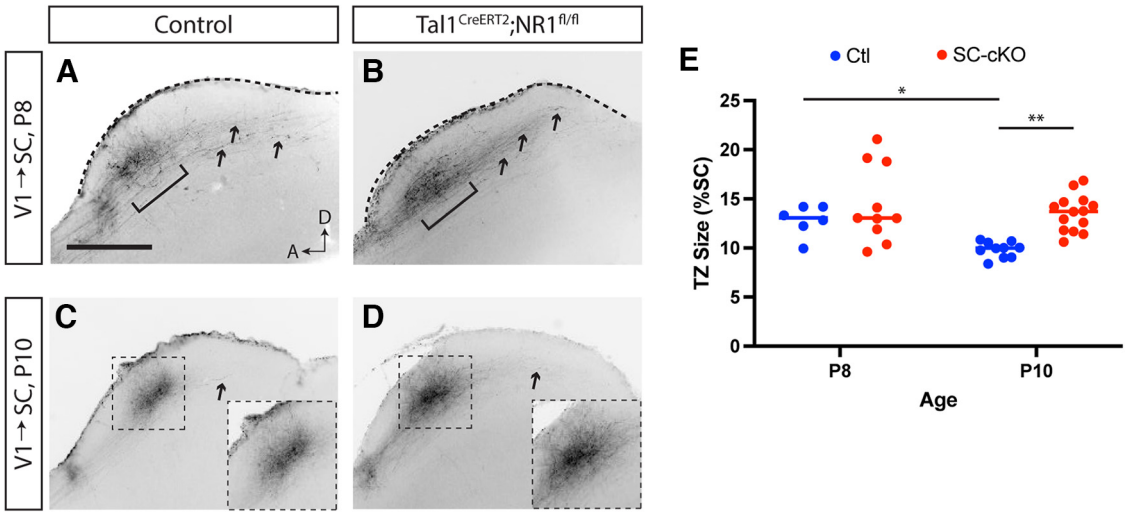

Figure 7. Impaired refinement of corticocollicular axon terminals in *GluN1* SC-cKO mice. ***A***, ***B***, Parasagittal sections through the SCs of P8 control (***A***) and *Tal1*^{CreERT2};*GluN1*$^{fl/fl}$ mice administered tamoxifen from P6 to P8 reveal termination zones of labeled corticocollicular axons and several unrefined axon terminals (arrow). Scale bar, 500 mm. A, Anterior; D, dorsal. ***C***, ***D***, Parasagittal sections through the SCs of P10 control (***C***) and *Tal1*^{CreERT2};*GluN1*$^{fl/fl}$ mice (***D***) administered tamoxifen from P6 to P8 reveal TZs of labeled corticocollicular axons and a few unrefined axon terminals (arrow). Insets, Enlargements of the regions indicated in dashed boxes. ***E***, Quantification of corticocollicular TZ size as a percent of the SC at P8 and P10 reveals a significant decrease from P8 to P10 in Ctl mice and a significant increase at P10 in *GluN1* SC-cKO mice. Lines indicate median. *$p < 0.05$; **$p < 0.01$; two-way ANOVA with Sidak's multiple comparisons test.

regulated recombination in multiple neuronal subtypes in the sSC. When we used this line to ablate GluN1 expression beginning at P6, we found enlarged corticocollicular terminal fields and a failure to refine. Importantly, the retinocollicular map in this model was unaffected, suggesting disrupted map alignment. Together, these data demonstrate a novel role for collicular NMDARs in visual map alignment and support the hypothesis that correlated activity between retinal and cortical inputs in the SC mediate visual map alignment.

NMDARs expressed by Tal1^{+} neurons are required for L5-V1 projection refinement in the SC

Leveraging the temporal control provided by the *Tal1*^{CreERT2} line, we were able to test the hypothesis that visual map alignment in

the sSC is dependent on postsynaptic NMDARs. To begin, we showed that ablation of NMDAR function in Tal1$^+$ neurons beginning at P6 did not alter retinocollicular topography. These data suggest that NMDARs expressed by postsynaptic neurons in the SC are not required to maintain topographic order of retinocollicular projections after it is initially established. An alternative possibility is that RGCs simply do not innervate Tal1$^+$ neurons in the SC, and no phenotype is observed as a result. Given the broad recombination in the sSC, we observed in *Tal1*^{CreERT2} mice, we feel this alternative is unlikely. However, cell type-specific transsynaptic tracing experiments are needed to distinguish these possibilities. Importantly, we performed our analysis of retinocollicular mapping at P12, leaving open the question of whether NMDARs are required for maintenance of topographic order in the retinocollicular projection beyond this time point.

Next, we found that ablation of NMDAR function in Tal1$^+$ neurons beginning at P6 resulted in disrupted and enlarged, and in some cases duplicated, L5-V1 TZs in the sSC. Together with our finding of an intact retinocollicular map, these data suggest that map alignment is disrupted in the absence of NMDAR function. Time-course studies suggest this is because of a lack of refinement of L5-V1 axons, consistent with a role for NMDARs in detecting coincident activity and initiating synaptic strengthening. Intriguingly, while these data support an activity-dependent mechanism underlying retinal instruction of visual map alignment, we did observe that a subset of our tracings resulted in duplicated TZs, reminiscent of prior work in *Isl2*^{EfnA3} knock-in mice (Savier et al., 2017). How this duplication arises in SC-cKO mice remains unclear. One possibility is that ephrin-As expressed on RGC terminals and NMDARs expressed on SC neuron dendrites may participate in a common pathway driving appropriate termination and alignment. Indeed, previous work suggests that ephrin-A/EphA interactions mediate NMDAR-containing synaptogenesis in the developing hippocampus (Akaneya et al., 2010), providing one potential route of cross-talk between these pathways. Alternatively, duplicated TZs could reflect distinct populations of L5-V1 neurons innervating Tal1$^+$ and Tal1$^-$ SC neurons, with the latter able to establish a condensed TZ. The reduced penetrance of this phenotype could be driven by stochastic forces that appear to operate at the microscale in the establishment of topography in the SC (Owens et al., 2015).

Another intriguing finding from these experiments is the apparent specificity of GluN1 requirement in Tal1$^+$ neurons in the SC. While our data suggest that *Tal1* is widely expressed in the sSC and in a diverse array of neuronal subtypes, it is by no means expressed by all neurons. We posit two mechanisms by which deletion of GluN1 in only Tal1$^+$ neurons could play such a critical role in visual map alignment. First, NMDARs could be functioning as coincidence detectors in Tal1$^+$ neurons receiving inputs from both RGCs and L5-V1 neurons at similar topographic positions in the retina and V1, respectively. In support of this, trans-synaptic anterograde tracing suggests that L5-V1 neurons can innervate both excitatory and inhibitory neurons in the SC, exhibiting a slight preference for the former (Zingg et al., 2017). Thus, it is possible that enough L5-V1 neurons innervate Tal1$^+$ neurons in the SC that our DiI tracing paradigm detects deficits specific to this subpopulation. Experiments leveraging the *Tal1*^{CreERT2} line to specifically label presynaptic partners are needed to resolve this question. A second possibility is that Tal1$^+$ neurons play a role in the propagation of spontaneous waves of activity in the developing SC, and that *GluN1* expression is critical for this function. While retinal waves are efficiently transferred to the SC and require action potential propagation by RGCs (Ackman et al., 2012), whether local circuits in the SC modify waves is unclear. Future studies examining wave propagation in the retina, SC and V1 in the presence and absence of collicular GluN1 are needed to address this possibility.

Tal1^{CreERT2} line allows for gene manipulation in the sSC with temporal control

Compared with other visual regions, such as the retina and V1, the genetic tools available to manipulate gene expression in the SC are relatively limited. cKO studies of relative contributions of RGCs and SC neurons during topographic mapping have relied on the well-established En1^{Cre} line (Burbridge et al., 2014; Suetterlin and Drescher, 2014), which is expressed broadly from the midbrain–hindbrain boundary beginning early in development (Kimmel et al., 2000). Additional lines have recently been characterized, which mark distinct neuronal populations in the SC and regulate specific aspects of behavior (Gale and Murphy, 2014; Hoy et al., 2019). A limitation of all these lines is a lack of temporal control over recombination. Other groups developed tamoxifen-inducible lines driven by promoter elements of the *Tal1* gene (Bradley et al., 2007); however, initial reports suggested a small degree of recombination in the absence of tamoxifen administration, which we confirmed (data not shown), limiting the precision of temporal control.

Here, we generated a new animal model (*Tal1*^{CreERT2}) to overcome these difficulties and allow for recombination in neurons of the midbrain and sSC with tight temporal regulation. The T-cell acute lymphocytic leukemia 1 (*Tal1*) gene, also referred to as the stem cell leukemia (*SCL*) gene, is a master regulator of hematopoiesis and plays an important role in angiogenesis (Begley and Green, 1999; Lécuyer and Hoang, 2004; Göthert et al., 2005). Interestingly, the *Tal1* gene within the brain is restricted to neurons in the midbrain, hindbrain, and the lateral and caudal thalamic region (van Eekelen et al., 2003; Bradley et al., 2006). Of note, in addition to recombination in neurons in the sSC, we also found sparse recombination in the LGN, with recombination in neuropil limited to the vLGN and intergeniculate leaflet. These data are consistent with previous studies of an *SCL*^{LacZ} knock-in (Elefanty et al., 1999), a Cre transgenic line based on neuron-specific enhancers (Bradley et al., 2007), and mRNA expression (Lee et al., 2017). Similarly, we observed substantial recombination in putative hematopoietic and endothelial lineages, consistent with the known role of *Tal1* in specification of these lines. Interestingly, the pattern of blood vessel staining was reduced when tamoxifen was administered at later ages in our hands. However, we could not distinguish whether this was because of reduced expression in mature endothelial cells or inefficient activation of CreERT2 in these lineages at relatively lower doses.

Consistent with previous studies, we found that *Tal1*^{CreERT2} mice mark predominantly neurons in the sSC; and expression was restricted to Tal1$^+$ cells, as expected based on the construct design. Previous studies suggest that *Tal1* expression is closely associated with GABAergic markers in the developing ganglionic eminences and may regulate inhibitory neuron fate in the midbrain, tegmentum, and substantia nigra (Achim et al., 2013; Morello et al., 2020). Somewhat in contrast, our data suggest that Tal1$^+$ neurons in the sSC are comprised of both excitatory and inhibitory subpopulations. Interestingly, neither parvalbumin$^+$ nor neurogranin$^+$ neurons in the sSC are marked in *Tal1*^{CreERT2} mice, but ~30% of marked neurons are Reelin$^+$. While Reelin

has been shown to play important roles in establishing lamination, myelination patterns, and ipsilateral RGC targeting in the sSC (Baba et al., 2007; Antonioli-Santos et al., 2017), little is known about the function of Reelin$^+$ neurons. In the forebrain, Reelin is expressed primarily in interneurons and colocalized with a variety of subpopulation markers (Alcántara et al., 1998; Pesold et al., 1998). Overall, our data suggest that Tal1$^+$ neurons comprise a substantial portion of all neurons in the sSC (~30%), but future studies are needed to characterize the function and heterogeneity of this population.

In conclusion, in this study, we used a novel cKO animal to understand the role of NMDARs expressed in the SC during the period of visual map alignment. *Tal1^{CreERT2}* mice allow for temporally controlled gene manipulation in a broad population of neurons in the sSC and throughout much of the midbrain. Inducing ablation of *GluN1* beginning at P6 did not alter retinocollicular map organization but did disrupt corticocollicular projection refinement. These data demonstrate that NMDAR function in Tal1$^+$ neurons in the SC is required for establishment of corticocollicular circuitry, and suggest they mediate activity-dependent retinal instruction of visual map alignment.

References

Achim K, Peltopuro P, Lahti L, Tsai HH, Zachariah A, Astrand M, Salminen M, Rowitch D, Partanen J (2013) The role of Tal2 and Tal1 in the differentiation of midbrain GABAergic neuron precursors. Biol Open 2:990–997.

Ackman JB, Burbridge TJ, Crair MC (2012) Retinal waves coordinate patterned activity throughout the developing visual system. Nature 490:219–225.

Akaneya Y, Sohya K, Kitamura A, Kimura F, Washburn C, Zhou R, Ninan I, Tsumoto T, Ziff EB (2010) Ephrin-A5 and EphA5 interaction induces synaptogenesis during early hippocampal development. PLoS One 5:e12486.

Alcántara S, Ruiz M, D'Arcangelo G, Ezan F, de Lecea L, Curran T, Sotelo C, Soriano E (1998) Regional and cellular patterns of reelin mRNA expression in the forebrain of the developing and adult mouse. J Neurosci 18:7779–7799.

Antonioli-Santos R, Lanzillotta-Mattos B, Hedin-Pereira C, Serfaty CA (2017) The fine tuning of retinocollicular topography depends on reelin signaling during early postnatal development of the rat visual system. Neuroscience 357:264–272.

Baba K, Sakakibara S, Setsu T, Terashima T (2007) The superficial layers of the superior colliculus are cytoarchitectually and myeloarchitectually disorganized in the reelin-deficient mouse, reeler. Brain Res 1140:205–215.

Basso MA, May PJ (2017) Circuits for action and cognition: a view from the superior colliculus. Annu Rev Vis Sci 3:197–226.

Basso MA, Bickford ME, Cang J (2021) Unraveling circuits of visual perception and cognition through the superior colliculus. Neuron 109:918–937.

Begley CG, Green AR (1999) The SCL gene: from case report to critical hematopoietic regulator. Blood 93:2760–2770.

Bradley CK, Takano EA, Hall MA, Göthert JR, Harvey AR, Begley CG, van Eekelen JA (2006) The essential haematopoietic transcription factor Scl is also critical for neuronal development. Eur J Neurosci 23:1677–1689.

Bradley CK, Takano EA, Göthert JR, Göttgens B, Green AR, Begley CG, van Eekelen JA (2007) Temporal regulation of Cre-recombinase activity in Scl-positive neurons of the central nervous system. Genesis 45:145–151.

Burbridge TJ, Xu H, Ackman JB, Ge X, Zhang Y, Ye MJ, Zhou ZJ, Xu J, Contractor A, Crair MC (2014) Visual circuit development requires patterned activity mediated by retinal acetylcholine receptors. Neuron 84:1049–1064.

Cang J, Rentería RC, Kaneko M, Liu X, Copenhagen DR, Stryker MP (2005) Development of precise maps in visual cortex requires patterned spontaneous activity in the retina. Neuron 48:797–809.

Cline HT, Constantine-Paton M (1989) NMDA receptor antagonists disrupt the retinotectal topographic map. Neuron 3:413–426.

Elefanty AG, Begley CG, Hartley L, Papaevangeliou B, Robb L (1999) SCL expression in the mouse embryo detected with a targeted lacZ reporter gene demonstrates its localization to hematopoietic, vascular, and neural tissues. Blood 94:3754–3763.

Gale SD, Murphy GJ (2014) Distinct representation and distribution of visual information by specific cell types in mouse superficial superior colliculus. J Neurosci 34:13458–13471.

Göthert JR, Gustin SE, Hall MA, Green AR, Göttgens B, Izon DJ, Begley CG (2005) In vivo fate-tracing studies using the Scl stem cell enhancer: embryonic hematopoietic stem cells significantly contribute to adult hematopoiesis. Blood 105:2724–2732.

Hoy JL, Bishop HI, Niell CM (2019) Defined cell types in superior colliculus make distinct contributions to prey capture behavior in the mouse. Curr Biol 29:4130–4138.e5.

Johnson KO, Triplett JW (2021) Wiring subcortical image-forming centers: topography, laminar targeting, and map alignment. Curr Top Dev Biol 142:283–317.

Kesner P, Schohl A, Warren EC, Ma F, Ruthazer ES (2020) Postsynaptic and presynaptic NMDARs have distinct roles in visual circuit development. Cell Rep 32:107955.

Kimmel RA, Turnbull DH, Blanquet V, Wurst W, Loomis CA, Joyner AL (2000) Two lineage boundaries coordinate vertebrate apical ectodermal ridge formation. Genes Dev 14:1377–1389.

Kutsarova E, Munz M, Ruthazer ES (2016) Rules for shaping neural connections in the developing brain. Front Neural Circuits 10:111.

Lécuyer E, Hoang T (2004) SCL: from the origin of hematopoiesis to stem cells and leukemia. Exp Hematol 32:11–24.

Lee B, Lee M, Song S, Loi LD, Lam DT, Yoon J, Baek K, Curtis DJ, Jeong Y (2017) Specification of neurotransmitter identity by Tal1 in thalamic nuclei. Dev Dyn 246:749–758.

Madisen L, Zwingman TA, Sunkin SM, Oh SW, Zariwala HA, Gu H, Ng LL, Palmiter RD, Hawrylycz MJ, Jones AR, Lein ES, Zeng H (2010) A robust and high-throughput Cre reporting and characterization system for the whole mouse brain. Nat Neurosci 13:133–140.

May PJ (2006) The mammalian superior colliculus: laminar structure and connections. Prog Brain Res 151:321–378.

McLaughlin T, Torborg CL, Feller MB, O'Leary DD (2003) Retinotopic map refinement requires spontaneous retinal waves during a brief critical period of development. Neuron 40:1147–1160.

Morello F, Borshagovski D, Survila M, Tikker L, Sadik-Ogli S, Kirjavainen A, Estartús N, Knaapi L, Lahti L, Törönen P, Mazutis L, Delogu A, Salminen M, Achim K, Partanen J (2020) Molecular fingerprint and developmental regulation of the tegmental GABAergic and glutamatergic neurons derived from the anterior hindbrain. Cell Rep 33:108268.

Nicoll RA, Malenka RC (1999) Expression mechanisms underlying NMDA receptor-dependent long-term potentiation. Ann NY Acad Sci 868:515–525.

Owens MT, Feldheim DA, Stryker MP, Triplett JW (2015) Stochastic interaction between neural activity and molecular cues in the formation of topographic maps. Neuron 87:1261–1273.

Pesold C, Impagnatiello F, Pisu MG, Uzunov DP, Costa E, Guidotti A, Caruncho HJ (1998) Reelin is preferentially expressed in neurons synthesizing gamma-aminobutyric acid in cortex and hippocampus of adult rats. Proc Natl Acad Sci USA 95:3221–3226.

Ramos-Moreno T, Galazo MJ, Porrero C, Martínez-Cerdeño V, Clascá F (2006) Extracellular matrix molecules and synaptic plasticity: immunomapping of intracellular and secreted Reelin in the adult rat brain. Eur J Neurosci 23:401–422.

Savier E, Eglen SJ, Bathelemy A, Perraut M, Pfrieger FW, Lemke G, Reber M (2017) A molecular mechanism for the topographic alignment of convergent neural maps. Elife 6:e20470.

Savier EL, Dunbar J, Cheung K, Reber M (2020) New insights on the modeling of the molecular mechanisms underlying neural maps alignment in the midbrain. Elife 9:e59754.

Schindelin J, Arganda-Carreras I, Frise E, Kaynig V, Longair M, Pietzsch T, Preibisch S, Rueden C, Saalfeld S, Schmid B, Tinevez JY, White DJ, Hartenstein V, Eliceiri K, Tomancak P, Cardona A (2012) Fiji: an open-source platform for biological-image analysis. Nat Methods 9:676–682.

Schmittgen TD, Livak KJ (2008) Analyzing real-time PCR data by the comparative C(T) method. Nat Protoc 3:1101–1108.

Simon DK, Prusky GT, O'Leary DD, Constantine-Paton M (1992) N-methyl-D-aspartate receptor antagonists disrupt the formation of a mammalian neural map. Proc Natl Acad Sci USA 89:10593–10597.

Soriano P (1999) Generalized lacZ expression with the ROSA26 Cre reporter strain. Nat Genet 21:70–71.

Suetterlin P, Drescher U (2014) Target-independent ephrinA/EphA-mediated axon-axon repulsion as a novel element in retinocollicular mapping. Neuron 84:740–752.

Tikidji-Hamburyan RA, El-Ghazawi TA, Triplett JW (2016) Novel models of visual topographic map alignment in the superior colliculus. PLoS Comput Biol 12:e1005315.

Triplett JW, Owens MT, Yamada J, Lemke G, Cang J, Stryker MP, Feldheim DA (2009) Retinal input instructs alignment of visual topographic maps. Cell 139:175–185.

Tsien JZ, Huerta PT, Tonegawa S (1996) The essential role of hippocampal CA1 NMDA receptor-dependent synaptic plasticity in spatial memory. Cell 87:1327–1338.

van Eekelen JA, Bradley CK, Göthert JR, Robb L, Elefanty AG, Begley CG, Harvey AR (2003) Expression pattern of the stem cell leukaemia gene in the CNS of the embryonic and adult mouse. Neuroscience 122:421–436.

Wang Q, Burkhalter A (2013) Stream-related preferences of inputs to the superior colliculus from areas of dorsal and ventral streams of mouse visual cortex. J Neurosci 33:1696–1705.

Zingg B, Chou XL, Zhang ZG, Mesik L, Liang F, Tao HW, Zhang LI (2017) AAV-mediated anterograde transsynaptic tagging: mapping corticocollicular input-defined neural pathways for defense behaviors. Neuron 93:33–47.